PAPER • OPEN ACCESS

Satellite-based landslide distribution mapping with the adoption of deep learning approach in the Kuantan River Basin, Pahang

View the article online for updates and enhancements.

Satellite-based landslide distribution mapping with the adoption of deep learning approach in the Kuantan River Basin, Pahang

Nur Aqilah Yusri[1], Syarifuddin Misbari[1,*], Izza Wajihah Ismail[1] and Jacqueline Isabella Anak Gisen[1]

[1]Faculty of Civil Engineering Technology (FCET), Universiti Malaysia Pahang Al-Sultan Abdullah, Lebuh Persiaran Tun Khalil Yaakob, 26300 Gambang, Pahang

Corresponding e-mail: syarifuddinm@umpsa.edu.my

Landslides are one of the major geological phenomena that is widespread across the globe and have caused destructive outcomes to human life and the overall economic system. Tedious work is required to conventionally collect all evidence of multiple sizes of landslide occurrences in such a huge, developing city, including the Kuantan River Basin (KRB). In fact, landslides are difficult to identify in remote areas, such as in thick and mountainous areas, if no aerial devices or sensor technology is provided at the incident area. Ironically, the landslide distribution map is a useful tool that helps in staging the landslide mitigation plan for landslide-prone areas. Thus, the objectives of this study are (i) to identify landslide events using deep learning and vegetation index approaches on optical satellite data; and (ii) to develop landslide distribution mapping in KRB using the best approach. Remotely sensed optical images of Landsat 8 OLI and Worldview-2 were used to map the landslide distribution and study the spectral pattern of the landslide area. Normalized Difference Vegetation Index (NDVI) were generated for two consecutive years, which is from the year 2022 to 2023. Spectral bands in red and infrared are used to generate the NDVI for visual interpretation of landslide occurrences. The deep learning based on Convolutional Neural Network (CNN) model were used for the pixel classification process. The main output of this study would be a landslide distribution map for the KRB area with high accuracy. The result has also been verified using drone monitoring at the incident sites, which was able to improve landslide detection in tropical environments. Landslide distribution maps accuracy was measured by using the ROC-AUC method, the map accuracy is 88.9%. This map should help the government and private sector plan for the city's urban development and provide proper planning for geohazard mitigation. An accurate landslide distribution map could be a source of reference for the National Disaster Management Authority (NADMA) for a quick rescue during emergency.

Keywords: Deep learning, vegetation index, NDVI, Landsat 8, WorldView-2, ROC-AUC

1. Introduction

Landslide is a major geological hazard that is widespread around the globe and has caused negative impact to human life, destruction to infrastructure and affect the overall economic system [1]. World Health Organization (WHO) recorded 378 major landslide activities that occurred worldwide between 1998-2017. Between these years, a total of 4.8 million people were affected by the landslide hazard, and this has caused

18,414 deaths. The severe outcomes of landslide activity have caused economic degradation, losses of life, changes in land morphology, and damage to building structures, roads, and other facilities. The fatalities resulting from landslide activity can be minimized by having a strategic landslide mitigation plan. Thus, having a landslide distribution map can be a critical source of information for landslide risk analysis, which would benefit the public, and private sectors, governmental departments, and scientific community on local and international scales.

Landslide distribution maps store the location information, date, and types of landslide occurrences [2]. There are many techniques that can be applied to generate a landslide distribution map, the selection of these techniques relies on the scale, extent of the study area, resolution, the purpose of the landslide mapping, and data availability [3]. The conventional methods for mapping landslide distribution are the visual interpretation of stereoscopic aerial photographs and geomorphological field mapping [4]. The geomorphological field mapping is a reliable method to map the landslide distribution, however, this method is time-consuming and consumes a lot of expense and manpower. As for the visual interpretation of the aerial photograph, this method remains widely adopted in the landslide distribution mapping due to its flexibility and data availability. The visual interpretation method is fully relying on the experience of the geomorphologist to detect the presence of a landslide, the process is inexpensive and subjective to the geomorphologist's evaluation. The new methods and technologies that facilitate landslide mapping are the study of surface morphology using a high-resolution digital elevation model (DEM), the interpretation of satellite images, and the use of advanced tools such as GIS software to expedite the mapping process.

When mapping the landslide distribution for the study area, there are a few factors that need to be considered, which are the size of the landslide, type of the landslide, morphology, and topography of the area. To identify the size of the landslide event, the guidelines from the Global Landslide Catalog (GLC) were used. GLC has been created by NASA Goddard Space Flight Centre since 2007, with the aim of selecting landslide events that was triggered by rainfall from all over the world, regardless of magnitude, effects, or location. The GLC considers all categories of mass movements related to rainfall that have been recorded by media, disaster databases, scientific publications, or other sources [5,6]. GLC has divided the landslide event into five classifications based on their size and impact, the classes can be seen in Table 1.

Continuous advancement of remote sensing technologies has made the process of acquiring high-resolution optical satellite images more accessible. It is now easier to acquire images for pre and post event, which helps to improve the generation of landslide inventory maps [7–10]. The usage of Geographic Information System (GIS) technology also helps to improve the process of landslide distribution mapping. The capability of the GIS technology to process large volumes of spatial data and integrate with the remotely sensed data will facilitate the generation of the landslide distribution map [11]. GIS technology will help to create a spatial database that contains the landslide information of the area, continuous update on the database will help to generate an up-to-date landslide distribution map for the area, which will be useful for land management and risk mitigation.

Using the available satellite images, the normalized difference vegetation index (NDVI) can be generated to map the landslide distribution in the area. NDVI is a widely used remote sensing technique to monitor and assess vegetation health and density. Regular monitoring of NDVI over time can help identify gradual changes in vegetation patterns that might be associated with unstable terrain. Landslide-prone areas might exhibit a decrease in NDVI values due to stress on vegetation caused by soil movement or gradual slope changes. By implementing a temporal data analysis for observing the NDVI value for an area, the landslide distribution map can be created by identifying areas with decreasing NDVI values. However, this method is limited to a vegetated region and not suitable for less vegetated areas.

World Sustainable Construction Conference 2023

IOP Conf. Series: Earth and Environmental Science   1296 (2024) 012014

IOP Publishing

doi:10.1088/1755-1315/1296/1/012014

Table 1: Landslide classification guide [12].

Size	Descriptions	Volume (meter)
Small	Small landslides affect one hillslope or small area. One road is blocked, cleaned in a few hours. No fatalities	< 2.154 m
Medium	Moderate size landslide, a single or multiple events within a region, destruct a large amount of material. Road is blocked for multiple days, multiple roads blocked, multiple houses damaged, at least one fatality.	2.154 to < 10 m
Large	Multiple landslides events in one place but cover a wide area. Mild destruction to infrastructure and roads, moderate to high numbers of fatalities. Tens to hundreds of people need to be displaced.	10 to < 21.54 m
Very Large	Very large or multiple events landslide that affect entire region. High number of fatalities.	21.54 to <100 m
Catastrophic	Catastrophic impact to infrastructure and roads. Multiple roads, village and towns buried. Tens of thousands of people may be displaced. Hundreds to thousands of fatalities.	>100 m

Nowadays the popular method to detect landslide events is by using Artificial Intelligence (AI). AI-based technology helps to improve the visual interpretation method by implementing automatic object detection and pixel classification processes. Machine learning (ML) and deep learning (DL) are the AI-based technology that have proven to give reliable results in many geotechnical applications [13–17]. Deep learning is known as a subset of machine learning. It uses several layers of algorithms in the form of neural networks. The concept of data learning can be used to differentiate between ML and DL. In conventional ML, few steps are needed to train the data, the data need to go through pre-processing step, feature extraction, feature selection, learning and classification [18]. Through these processes, ML learn to find pattern in the data based on the available data, thus a biased feature selection may lead to incorrect discrimination between classes. Whereas DL able to run learning and classification simultaneously. In DL, the input data is analyzed through different layers of the network, with each layer defining specific features and patterns in the data. The difference between ML and DL can be seen in Figure 1.

Recurrent neural network (RNN) and convolutional neural network (CNN) are the most popular DL model that has been widely used in many applications and are excellent in handling big data [19]. Both DL models consist of layers, training parameters, and loss functions. To differentiate between CNNs model and RNNs model is based on the existence of additional convolutional and pooling layers in CNN [20], and by accepting only the current input data. On the other hand, RNN is able to accept previous input data and also the current input data [21]. For object detection and segmentation, the CNNs model has shown better results [22–24], whereas the RNNs model is better suited for image recognition and characterization [25]as well as temporal data analysis [26]. CNN have been proven to provide a higher success rate in object detection when a huge volume of training dataset was used for the model [23]. Aside from huge numbers of training

datasets, some other factor that also influence the performance of CNN model are the network architecture, machine's Graphic Processing Unit (GPU) capabilities, algorithms used in the model, and data augmentation [24] For image recognition, the application of conventional RNN with Long-Short Term Memory (LSTM) has been widely employed in the recent studies [25].

This paper discussed the application of DL and changes in vegetation index to identify the landslide events in Kuantan River Basin (KRB). Kuantan is the capital city of Pahang State, which received high volume precipitation during the Monsoon season in Malaysia. Northeast monsoon season occurred between November until March, during these months the east coast states of the peninsula, the northern part of Sabah, and the southern part of Sarawak are affected by heavy rains. Several landslide activities have been observed in this area due to the high precipitation received during the wet season. Despite the recurring landslide events, no landslide distribution map has been created for the study area. Thus, this research will generate landslide distribution map for the KRB area by utilizing the Landsat-8 optical image, WorldView-2 image, and GIS techniques. The objectives of this research are (i) to identify landslide events in KRB using deep learning and vegetation index approaches on optical satellite data; and (ii) to develop landslide distribution mapping in KRB using the best approach.
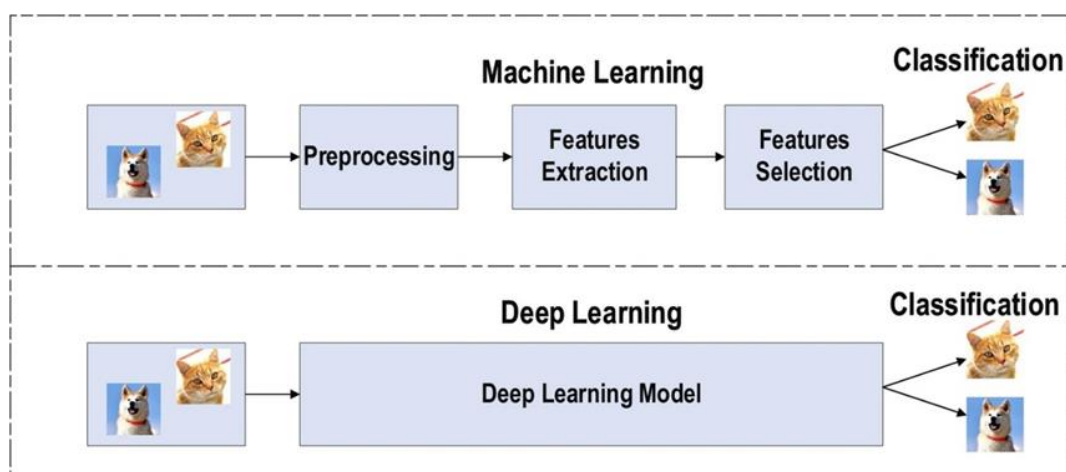

Figure 1: Illustration to demonstrate the difference between conventional ML and DL.

2.   Geology of the Study Area

The state of Pahang is located on Peninsular Malaysia's east coast, and Kuantan serves as its capital. The Kuantan River Basin (KRB) is a significant watershed that runs through the city. The basin has a total length of 86km with a drainage area that covers approximately 1638 km^2. Kuantan River is one of the largest rivers in peninsula Malaysia, sourcing from the Gunung Tapis, the water flow from Sg. Lembing to Sg. Kuantan is moving toward the southeast direction and discharging into the South China Sea. Along the Kuantan River, there are many tributaries namely as, Sg.Chereh, Sg.Galing, and Sg.Berapit. The Sg. Chereh and Chereh Dam cover the northeastern corner of the basin. Moving to the lower course of the river, there is a tributary called Sg. Gading. The map of the study area can be seen in Figure 2.

The carboniferous rock units that make up the research area's lithology primarily consist of phyllite, slate, shale, and sandstone. The northwest part of the study area is covered by the acid intrusive rock and Permian-Triassic limestone, while the bottom part of the study area is composed of a Quaternary rock unit, which is silt, clay, sand, peat, and minor gravel. Due to the geological location of the study area, KRB is

heavily affected during the Northeast Monsoon, which typically occurs from November until March. The northeastern part of Peninsular Malaysia (including the east coast) is affected by strong winds blowing from the northeast direction. These winds bring moist air and heavy rainfall from the South China Sea and the Pacific Ocean toward the eastern coastline of Peninsular Malaysia.
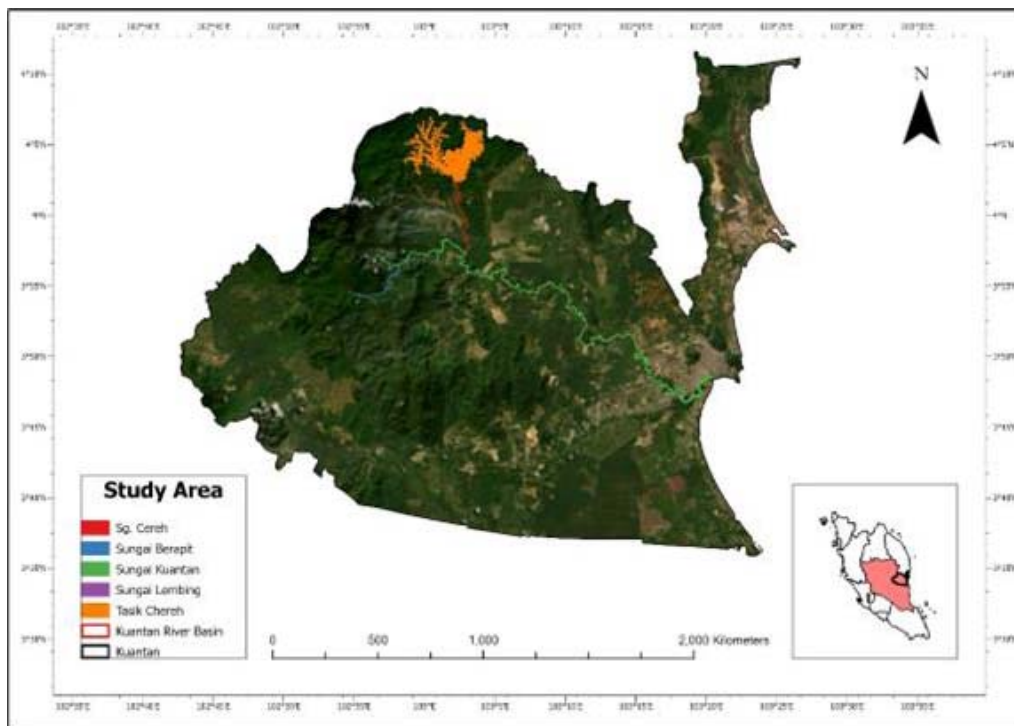

Figure 2: Map of the study area in Kuantan River Basin, Kuantan, Pahang.

3.   Materials and Methods

3.1   Data Acquisition
In preparation for this study, data are collected from multiple sources, the workflow of the research can be seen in Figure 3.

The primary data source for this research is mainly from the field visit, while the secondary data sources are from the satellite images and data supplied by the Malaysian departments. This study used Landsat-8 OLI, WorldView-2, and drone images to map the landslide distribution in the KRB area. Landsat-8 satellite carries OLI and Thermal Infrared sensors (TIRS) instruments. These two sensors provide a 30m resolution image for visible, near infrared, and shortwave infrared portions (VNIR, NIR, and SWIR), a 100m resolution for thermal images, and a 15m resolution for panchromatic. WorldView-2 provides a high-resolution image that captures 0.41m spatial resolution for panchromatic and 1.64m resolution for 8-band multispectral data. The characteristics of the Landsat-8 and WorldView-2 satellites can be seen in Table 2.

Table 2: Landsat-8 and WorldView-2 technical parameters.

| Technical parameter	Landsat-8 OLI	WorldView-2
Date launched	11th Feb 2013	8th October 2009
Orbit Altitude	705km	770km
Orbit Type	Sun-synchronous	Sun-synchronous
Revisit Time	16 days	Up to 1.1 days
Equator Crossing Time	nominally 10 AM (± 15 min.) local time (descending node)	10:30 am Descending node
Imaging Mode	15m Panchromatic 30m Multispectral bands 100m Thermal band	400-800 nm Panchromatic 450-800 nm Multispectral bands
Swath Width	185km	16.4 km
Data Quantization	16-bit	11-bit
Field of View (FOV)	14.7°	1.28°
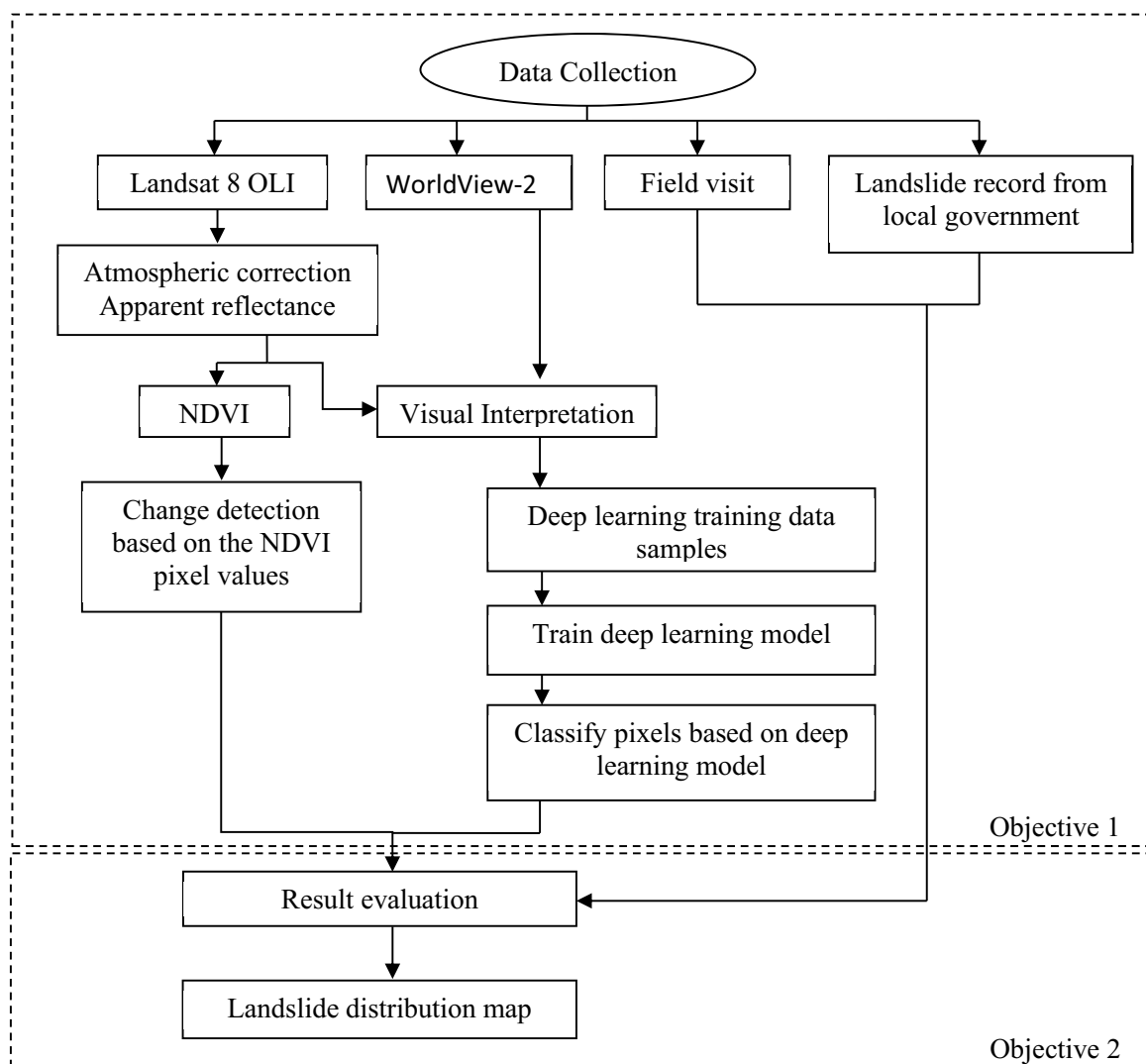
Figure 3: Research Workflow.

For the WorldView-2 image, the high-resolution image was purchased from a private company, the purchased imagery only covers some parts of Kuantan, which are the Sg.Lembing area and Gambang areas. The data specification for Landsat-8 and WorldView-2 can be seen in Table 3.

Table 3: Data specification for WorldView-2.

Technical Parameter	WorldView-2	
	Sg. Lembing	**Gambang**
Date Acquired	2021-11-09	2021-26-08
Number of Bands	4	4
Cloud Cover	0%	4%
Satellite Path direction	Full swath forward	-

Drone were used to capture images during the field visit. The drone model used in this research is DJI GL6D10A. Using drones is especially helpful in capturing images of large landslide areas, covering inaccessible areas, and providing high-resolution images of the landslide areas. An example of a landslide event that was captured using a drone can be seen in Figure 4.

The records of existing landslide events for the study area were obtained from the Malaysia Public Work Department (JKR). The data were obtained from the year 2021 to 2022. However, since the JKR department only handles geohazard events that occur near the road network, thus the data are limited to the road network area only. The data was supplied in the form of a vector point dataset with the XY location and date information.

Figure 4: Top view of landslide event at Taman Gambang Damai, Kuantan. This image was captured using drone DJI GL6D10A.

3.2   Landslide distribution map

To map the landslide distribution in the study area, two techniques were employed in this research, which are by observing the changes in vegetation index by using temporal data analysis and deep learning based on the CNN tool. Both methods were processed using the ArcGIS Pro software version 3.0.

3.2.1 *Normalized difference vegetation index (NDVI)*

NDVI is a widely used remote sensing technique to monitor and assess vegetation health and density. NDVI measure the reflectance value from two different bands, which are the near-infrared band (NIR) and red band. This method is very effective in a vegetative region but not suitable non-vegetated areas.

Two Landsat-8 images used to generate the NDVI were collected from the US Geological Survey Earth Resources Observation and Science Center [27]. The technical parameters for the Landsat 8 can be seen in Table 4.

Table 4: Technical specification for Landsat 8 OLI

Technical Parameter	Pre-monsoon	Post-monsoon
Date Acquired	19th June 2022	11th April 2023
Number of Bands	11 bands	11 bands
Processing level	L2SP	L2SP
Cloud Cover	5.47%	3.84%
Satellite Path direction	North-up	North-up

The Landsat 8 images were first pre-processed for the atmospheric correction and surface reflectance. Fast line-of-sight atmospheric analysis of the spectral hypercubes (FLAASH) algorithm were used for the atmospheric correction. This algorithm consists of the standard column water vapor amounts for each model atmosphere, this is based on the standard MODTRAN model atmosphere [27]. The Landsat 8 image were also pre-processed using the Apparent Reflectance function. The scene illumination and sensor-gain settings were used by the apparent reflectance tool to adjusts the reflectance value of Landsat-8 images. Two corrections were performed based on this function, which are; (1) the gain settings, the gain equation were reversed and the initial brightness values were re-build based on the image values (2) the scenes captured under different illumination scene were normalized in order to adjust the initial brightness values to a common lighting condition, this is based on the differences in sun angle and brightness. Even though the data type for the output image are the same as the input image, but the output image values are lower compared to the input value and clipped to the valid data range.

The analysis-ready Landsat-8 image will be used to create the NDVI by using the near-infrared and red bands of both datasets from the pre- and post-monsoon seasons. The formula used to create the NDVI can be seen in equation 1.

$$NDVI = (\boldsymbol{NIR - Red})/(\boldsymbol{NIR + Red}) \qquad (1)$$

To detect changes in NDVI value between the two raster images, the compute change raster tool in ArcGIS Pro were used to automatically detect the area that show changes in the pixel values. The compute change raster used the relative difference calculation that measure the difference in pixel values accounting for the quantities of the values being compared. The calculation used to calculate the relative difference can be seen in equation 2.

$$Output = \frac{(\boldsymbol{To\ raster - From\ raster})}{\boldsymbol{max(To\ raster, From\ raster)}} \qquad (2)$$

The existing landslide vector data was overlaid with the NDVI from year 2022 and 2023. The extract values to point tool were used to extract the vegetation pixel values for the landslide locations. The decline in the pixel value indicates that there is a loss of vegetation cover in that area potentially due to the landslide event. The NDVI value ranges from -1 to +1, where -0.5 to 0 indicates a water body, ≤ 0.1 indicate a barren area, sand or snow, between 0.2 to 0.3 represent grass and shrub area, and ≥ 0.5 indicate a densely vegetated area such as tropical rainforest [28].

3.2.2 Deep Learning Based on Convolution neural network (CNN)

DL technique can be categorized into three major group, which are unsupervised, semi-supervised and supervised [18]. The CNN model is categorized under deep supervised group along with RNN and deep neural network (DNN).

Landsat 8 OLI and WorldView-2 satellite images were used as the input data to create the training sample for DL. The training sample determine the performance of the CNN model, small training sample size can cause overfitting problems and weak classification ability, which will affect the CNN model performance. Thus, both images were used to create a satisfactory training sample dataset in order to improve the accuracy for the DL model. A polygon vector training sample dataset were created with class value of Landslide and Non-landslide locations. The labelled vector or raster and the remote sensing image were used as the input in the export training data for deep learning tool in ArcGIS Pro. This tool were used to create a deep learning training dataset by creating an image chips, that contain the feature or class of interest. The training dataset were used as the input data to train the model for DL.

The model training process will be based on the CNN architecture, which consist of three layers; (1) convolutional layer, (2) pooling layer and (3) fully connected layer. The basic architecture of CNN can be seen in Figure 5. The most significant layer in CNN is the convolutional layer, which responsible for features extraction. This layer contained set of convolutional filters, the input data will be pass through these filters to generate the output feature map. In convolution operation, kernel filter will be applied to the input data vertically and horizontally. In the convolutional stage, the dot product between the input image and the kernel is determined. The calculated dot product values represent the feature map of the output. The corresponding values from the dot product are multiplied and then summed up to create a single scalar value, calculated concurrently. This whole process will repeat until further sliding is no longer possible. The illustrated convolution operation can be seen in Figure 6.
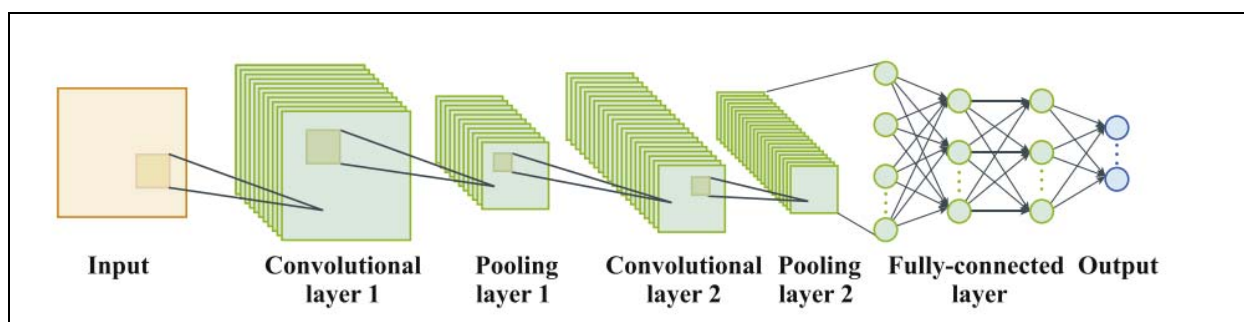

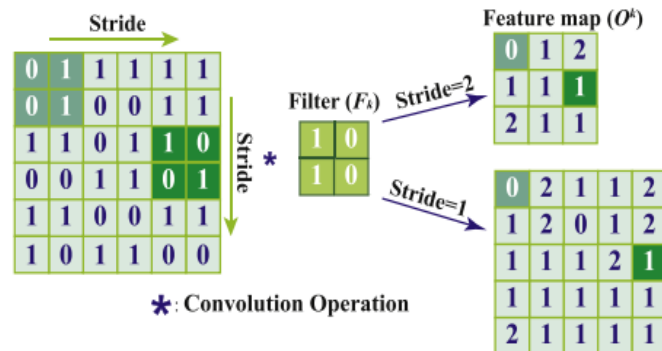**Figure 5**: Basic architecture of CNN [29]

Figure 6: Illustration of convolutional layer operation, the amount of movement between applied filters on the input is based on the stride [29].

Next stage is the pooling layer. In this stage, the most important factor is the sub-sampling of the feature maps. Pooling layer works on selecting the exact location of certain feature that was determined by the CNN from the input image. The shortcoming of pooling layer will cause the model to miss the relevant information and overall affecting the CNN model performance. Pooling layers create a smaller versions of large-scale feature maps but retain most of the significant data during the whole pooling stage. Prior to the pooling operation, the stride and the kernel are assigned with the original size, which are the same as in the convolutional process. There are different pooling strategies that can be used in each pooling levels, these strategies include global average pooling (GAP), global max pooling, global average pooling, gated pooling, and average pooling. The most popular and often used pooling techniques are the maximum, average and GAP. Figure 7 illustrate the three most popular pooling techniques.
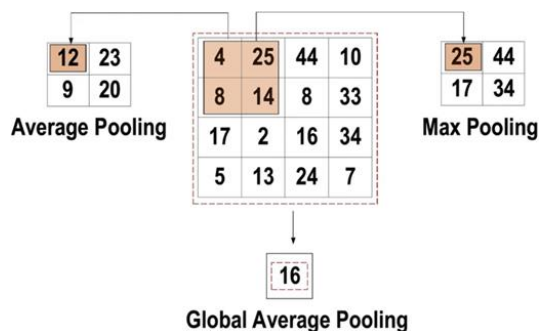

Figure 7: The example of pooling technique in CNN model

The last stage is the fully connected layer. This layer known as CNN's classifier. In this stage, every neuron is coupled to every neuron from the layer below, this technique is known as the Fully coupled (FC) technique. This layer is a feed-forward ANN, the operation is similar to a traditional multiple-layer perceptron neural network. The input for the FC layer were coming from the final pooling or convolutional layer. This input, which takes the shape of a vector, is made from the feature maps after they have been flattened. As shown in Figure 8, the output of the FC layer represents the final CNN output.
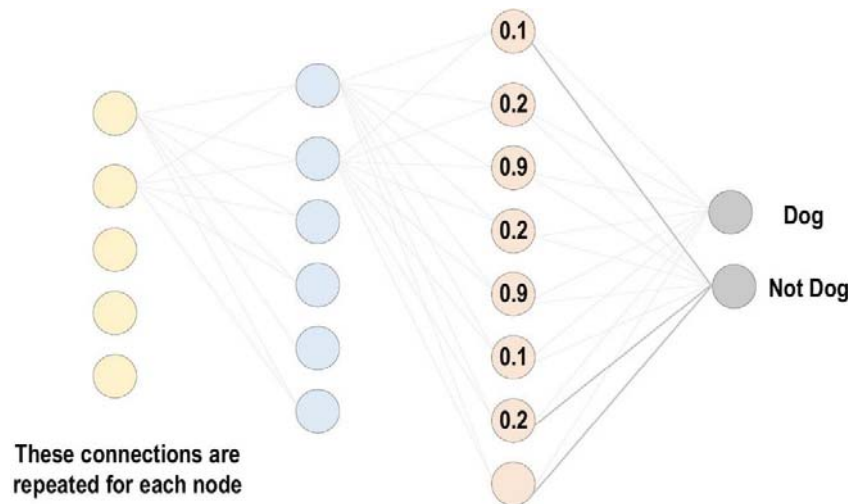
Figure 8: Illustration of fully connected layer[18]

For semantic segmentation, fully convolutional networks (FCNs) and their variants are popular CNN-based models [22]. FCNs have three key advantages over conventional CNNs, which are (1) retain spatial information; (2) reduce the required computing parameter; and (3) they enhance representational performance. FCNs substitute fully connected layers in the original CNNs with convolutional layers, which involve only convolutional (subsampling or up sampling) operations. The FCN model used in this research is the U-Net model. The train deep learning model tool will create a deep learning model package after completing the training process and provide the model evaluation performance information.

The resulted deep learning model package were used for the pixel classification process. The classify pixel based on deep learning tool will be used to classify the pixel based on the Landsat 8 OLI raster image. The input raster image used for the tool is from 11th April 2023. Python API (such as TensorFlow, PyTorch, or Keras) are the third-party deep learning function used by the classify pixel based on deep learning tool and the tool also uses the specified Python raster function to process each object.

4. Result

The deep learning and change in vegetation index approach were used in this study to map the landslide distribution in the KRB.

4.1 Result from vegetation index approach

Using the vegetation index approach, two NDVI was generated for the year 2022 and 2023. The resulted map from the computed change analysis between the two NDVIs can be seen in Figure 9. The pixel values for the historic landslide location were extracted from NDVI for the year 2022 and 2023, the decrease in pixel value represent the loss of vegetation cover in those areas. While the increase NDVI indicate that the historic landslide area has been covered by vegetation. The extracted NDVI pixel values can be seen in Table 5.

Table 5: The extracted NDVI pixel values from the historic landslide events. The shaded rows show the loss in vegetation from the year 2022 to 2023.

| OBJECTID	Pixel_2022	Pixel_2023
1	0.320511	0.277087
2	0.348945	0.188019
3	0.389126	0.378726
4	0.225641	0.25866
5	0.299294	0.285561
6	0.225641	0.25866
7	0.322967	0.338337
8	0.286471	0.266768
9	0.34507	0.318882
10	0.361951	0.364237
11	0.161609	0.366577
12	0.322966	0.305652
13	0.301916	0.316264
14	0.330262	0.316032
15	0.136763	0.180025
16	0.328154	0.276015
17	0.093671	0.115095
18	0.058276	0.121205
19	0.453069	0.410757
20	0.328776	0.327061
21	0.260548	0.26806
22	0.418105	0.338144
23	0.116859	0.15796
24	0.415445	0.263039
25	0.275444	0.343944
26	0.343991	0.35358
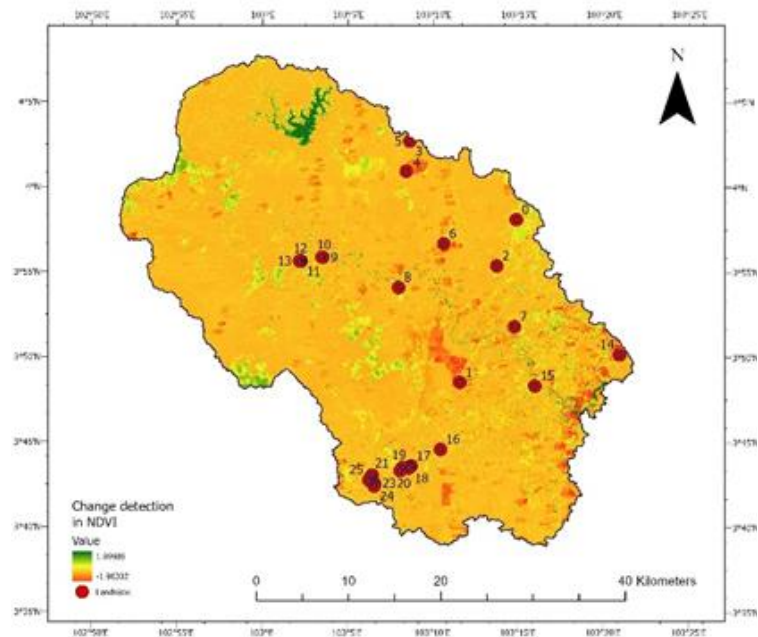
Figure 9: Landslide distribution map based on the changes in vegetation index from the year 2022 to 2023.

4.2   Deep learning based on CNN approach.

Based on the DL approach, a total of 1,118 training samples were generated for the whole area of Kuantan based on the Landsat 8 OLI and WorldView-2 image. 10% from the overall training samples were used as the validation sample to train the deep learning model. Figure 10 show the ground truth observed from the trained model.
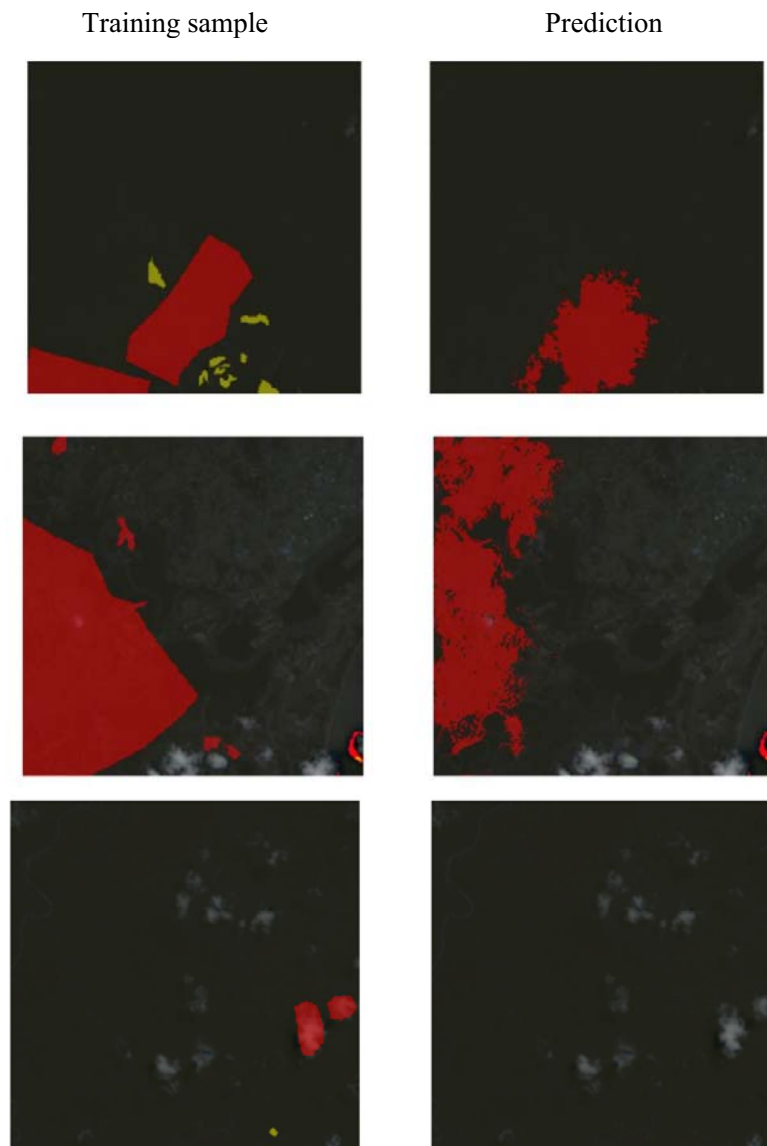
Training sample   Prediction

Figure 10: The ground truth resulted from the DL model.

As a result of the training, landslide distribution in KRB area was detected based on the Landsat 8 OLI satellite image. The example of the landslide location, training sample and the classified pixel based on the DL model are shown in Figure 11.
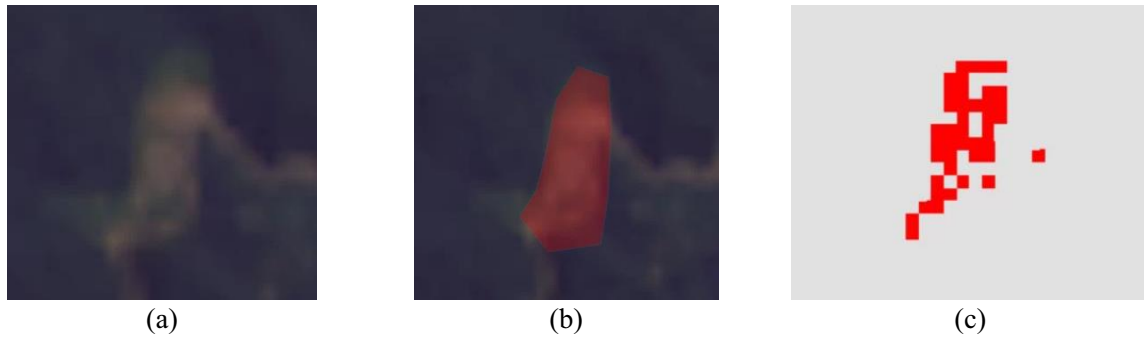
<div align="center">(a)   (b)   (c)</div>

Figure 11: (a) landslide location identified from Landsat 8 OLI. (b) Training sample created for DL. (c) Classified pixel detected based on the DL model.

The landslide distribution map resulted from the classified pixels based on the DL method can be seen in Figure 12.
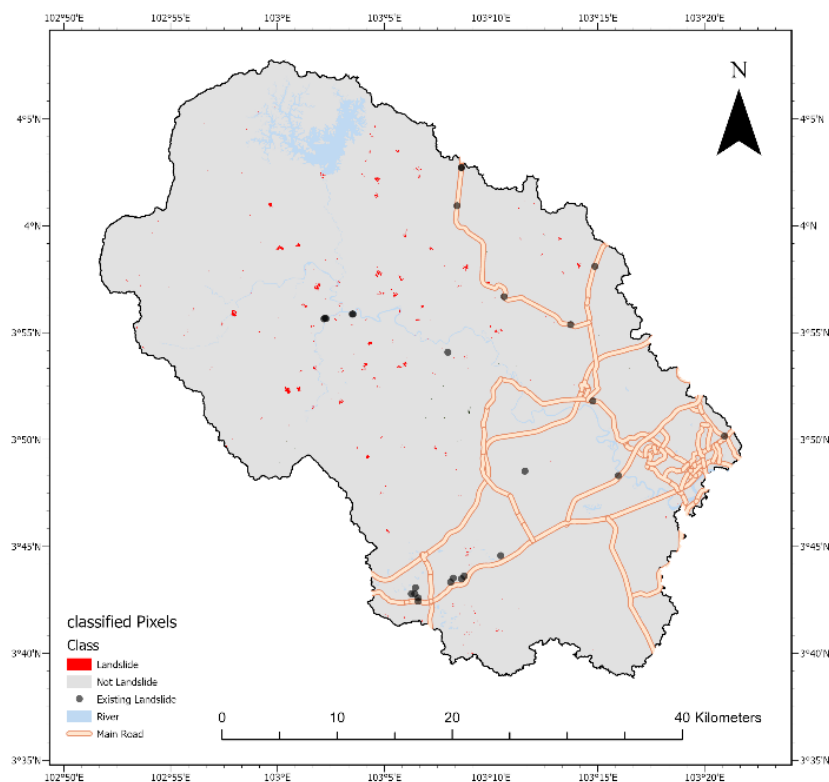

Figure 12: Landslide distribution map based on DL approach.

5. Accuracy Assessment

The Receiver Operating Characteristic (ROC) and the measurement for the Area Under the Curve (AUC) were applied to evaluate the results from the NDVI and deep learning approach. The AUC help to determine the reliability of the landslide distribution map produced by using the DL and NDVI approach. The ROC curve is drawn by X, which represents the false positive rate (1-specificity), and the Y axis, which represent

the true positive rate (sensitivity) [30]. Higher AUC value generally indicates a better-performing model in terms of discrimination between positive and negative classes. A good fit model has a range of values of ROC curve area between 0.5 to 1, any values that are below 0.5 represent a random fit model.

For the landslide distribution map generated using the NDVI approach, the area under the curve measurement is 0.651, which indicates that the map accuracy is 65.1 %. As for the landslide distribution map generated by using the DL method, the area under the curve measurement is 0.889, which indicates that the map accuracy is 88.9%. The ROC plot can be seen in Figure 13.
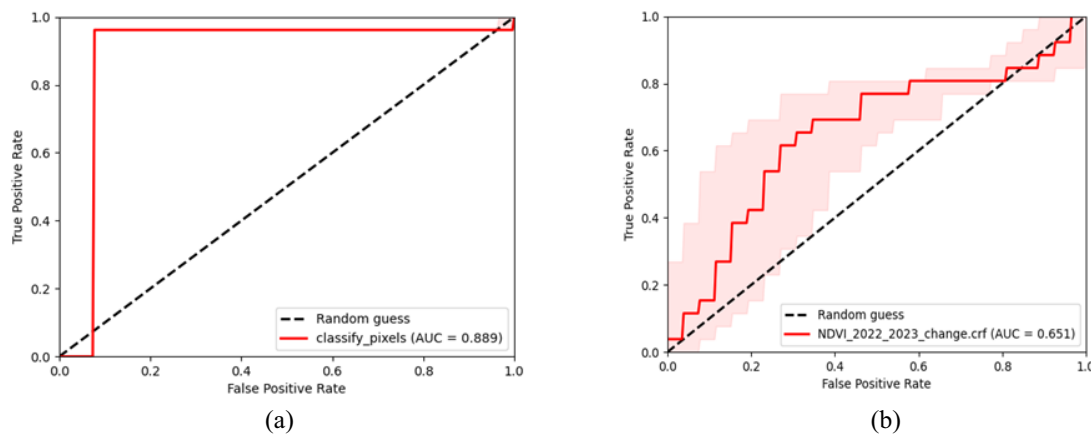

(a) (b)

Figure 13: (a) ROC plot for landslide distribution map from deep learning. (b) ROC plot for landslide distribution map from NDVI approach.

5.1 Deep learning model accuracy assessment

To evaluate the DL model, the pixel-based evaluation method was implemented in this study. The accuracy comparison is categorized into three group of classified pixels, which are the true positive (TP), false positive (FP) and false negative (FN). TPs represent the areas that are correctly identified as the landslide area. FP represent the areas that were determined as the landslide areas based on the classification but are not landslide by referring to the inventory dataset. Whereas FN determine the non-landslide areas. The quantitative evaluation for the resulted total areas of TP, FP and FN, three parameters were calculated in this research, which are, precision rate, recall rate and F1 score. Precision rates determine the number of exact landslides based on the classified areas. Recall rate was used to define the actual landslide location that were identified in the images. F1 score calculate the balance between the precision rate and recall rate. The precision rate, recall rate and F1 score were measured by using the equation 3, equation 4 and equation 5.

$$Precision\ rate = \frac{True\ positive}{(True\ positive + false\ positive)} \tag{3}$$

$$Recall\ rate = \frac{True\ positive}{(True\ positive + false\ negative)} \tag{4}$$

$$F1\ Score = \frac{2\ x\ precision\ x\ recall}{precision + recall} \tag{5}$$

The precision rate for the landslide areas from the DL model is 76.9%, while the recall rate 0.58 % and F1 score is 0.011. These values obtained from the DL can be seen in Table 6.

Table 6: Precision rate, recall rate and F1 score obtained from the DL model.

	Landslide	Non-landslide
Precision	0.769231	0.726162
Recall	0.005856	0.112806
F1 score	0.011624	0.195277

6. Discussion

Based on the two methods employed to map the landslide distribution in the KRB, DL based on the CNN method show higher accuracy compared to the changes in vegetation index method. Based on the historical landslide events, there are several landslides recorded within the urban areas at the south of the KRB area. Lacking vegetation cover in the urban area affect the accuracy for the changes in vegetation index method. Observing changes in vegetation index method is best employed in the vegetated region.

The existence of cloud in the Landsat 8 images used in this study also affect the accuracy of the generated NDVI. The least cloud cover image was chosen for this research, however, there are still some parts of the areas that are covered by cloud. When calculating the NDVI value for the satellite images, the area with cloud cover were classified as the bare land area, when running the compute change analysis tool to detect the changes in pixel values between the two NDVI, the clouds that was identified as the bare soil area were regarded as the area that has shown decrease in vegetation cover. Aside from the existence of cloud, the area that was used for agriculture purposes also affect the result of the changes in NDVI values. From the landslide distribution map generated using the changes in vegetation index, there are some areas in the middle part of KRB were marked as the areas that has shown decrease in vegetation cover. However, in the middle part of the KRB area are mostly covered by the agriculture area, thus the changes in vegetation index observed in these areas is not accurate.

For the second technique, which is the deep learning based on the CNN method, this method showed higher accuracy compared to the changes in vegetation index approach. However, the accuracy of DL is depending on the quantity of the training samples. Small training samples can cause the model to give an overfitting result. Higher amount of training samples used for the research will increase the accuracy and improve the DL model performance. The model architecture applied to CNN method also help to improve the reliability of the DL model. In this research, the U-Net pixel classification architecture were used for the image segmentation process. The U-Net pixel classification has been introduced in geological hazard analysis, which can produce an accurate segmentation for satellite images in detecting regional objects. The CNN based model with U-Net architecture provide a precision rate for detecting landslide up to 76.9%, 0.5 % recall rate and F1 score of 0.011. The obtained results suggest that the application of DL based on CNN and implementation U-Net architecture is suitable for the KRB area.

To validate the reliability of the landslide distribution map, ROC and AUC validation method was employed in this study. The AUC obtained using the change detection method in vegetation index approach is 65.0 %, while the AUC for the DL based on CNN method is 88.9%. Based on the accuracy assessment, the DL model provide more accurate landslide distribution map.

7. Conclusion

The DL model has proven to be more accurate compared to the changes in vegetation index approach. Thus the DL method would be the most suitable method to visualize the landslide distribution in the KRB area.The changes in vegetation approach are suitable to be applied in the area with tropical climate that vegetation cover. In the vegetated region, the changes in vegetation index approach can provide more

reliable results. CNN model with U-Net architecture has provide a good fit DL model for the KRB area. The accuracy of the model is highly depending on the availability of the training samples. Large size of training sample would create a good performance DL model. Since DL model has been a very popular method in landslide studies, more variant architecture has been derived and proposed for the landslide analysis. The implementation of DL model based on different model architecture should be considered to compare the suitability of the model with the KRB area. The training samples that has been created for the DL model should be continuously update, so that the samples can be used for DL model application in the future. An accurate landslide distribution map would benefit the local government, non-profit organization, local citizen to be aware of the landslide events and be prepared with a proper mitigation plan to reduce the loss resulting from the landslide hazard.

Acknowledgements

References

[1]   Nefeslioglu H A, Gokceoglu C and Sonmez H 2008 An assessment on the use of logistic regression and artificial neural networks with different sampling strategies for the preparation of landslide susceptibility maps *Engineering Geology* **97** 171–91

[2]   Guzzetti F, Mondini A C, Cardinali M, Fiorucci F, Santangelo M and Chang K-T 2012 Landslide inventory maps: New tools for an old problem *Earth Science Review* **112** 42–66

[3]   Mohan A, Singh A K, Kumar B and Dwivedi R 2021 Review on remote sensing methods for landslide detection using machine and deep learning *Transactions on Emerging Telecommunications Technologies* **32** 4

[4]   Mondini A C, Guzzetti F, Chang K-T, Monserrat O, Martha T R and Manconi A 2021 Landslide failures detection and mapping using Synthetic Aperture Radar: Past, present and future *Earth Science Review* **216** 103574

[5]   Kirschbaum D, Stanley T and Zhou Y 2015 Spatial and temporal analysis of a global landslide catalog *Geomorphology* **249** 4–15

[6]   Kirschbaum D B, Adler R, Hong Y, Hill S and Lerner-Lam A 2010 A global landslide catalog for hazard applications: method, results, and limitations *Natural Hazards* **52** 561–75

[7]   Travelletti J, Delacourt C, Allemand P, Malet J-P, Schmittbuhl J, Toussaint R and Bastard M 2012 Correlation of multi-temporal ground-based optical images for landslide monitoring: Application, potential and limitations *ISPRS Journal of Photogrammetry and Remote Sensing* **70** 39–55

[8]   Solari L, Del Soldato M, Montalti R, Bianchini S, Raspini F, Thuegaz P, Bertolo D, Tofani V and Casagli N 2019 A Sentinel-1 based hot-spot analysis: landslide mapping in north-western Italy *International Journal Remote Sensing* **40** 7898–921

[9]   Santangelo M, Marchesini I, Bucci F, Cardinali M, Fiorucci F and Guzzetti F 2015 An approach to reduce mapping errors in the production of landslide inventory maps *Natural Hazards and Earth System Sciences* **15** 2111–26

[10]	Casagli N, Cigna F, Bianchini S, Hölbling D, Füreder P, Righini G, Del Conte S, Friedl B, Schneiderbauer S, Iasio C, Vlcko J, Greif V, Proske H, Granica K, Falco S, Lozzi S, Mora O, Arnaud A, Novali F and Bianchi M 2016 Landslide mapping and monitoring by using radar and optical remote sensing: Examples from the EC-FP7 project SAFER *Remote Sensing Application* **4** 92–108

[11]	Roccati A, Paliaga G, Luino F, Faccini F and Turconi L 2021 GIS-Based Landslide Susceptibility Mapping for Land Use Planning and Risk Assessment *Land* **10** 162

[12]	Landslide reporter *Landslide Reporter Primer and Landslide Identification The Landslide Reporter's Guide*

[13]	Lo M K and Leung Y F 2019 Bayesian updating of subsurface spatial variability for improved prediction of braced excavation response *Canadian Geotechnical Journal* **56** 1169–83

[14]	Li X, Cheng X, Chen W, Chen G and Liu S 2015 Identification of Forested Landslides Using LiDar Data, Object-based Image Analysis, and Machine Learning Algorithms *Remote Sensing (Basel)* **7** 9705–26

[15]	Ching J and Phoon K-K 2019 Constructing Site-Specific Multivariate Probability Distribution Model Using Bayesian Machine Learning *J Engineering Mechanical* **145** 1

[16]	Papaioannou I and Straub D 2017 Learning soil parameters and updating geotechnical reliability estimates under spatial variability – theory and application to shallow foundations *Georisk: Assessment and Management of Risk for Engineered Systems and Geohazards* **11** 116–28

[17]	Zhang W, Li X, Xu T, Ma M, Zhang Y and Gao M Q 2016 Inflammatory responses of stromal fibroblasts to inflammatory epithelial cells are involved in the pathogenesis of bovine mastitis *Experimental Cell Research* **349** 45–52

[18]	Alzubaidi L, Zhang J, Humaidi A J, Al-Dujaili A, Duan Y, Al-Shamma O, Santamaría J, Fadhel M A, Al-Amidie M and Farhan L 2021 Review of deep learning: concepts, CNN architectures, challenges, applications, future directions *Journal of Big Data* **8** 53

[19]	Wang Y, Fang Z, Wang M, Peng L and Hong H 2020 Comparative study of landslide susceptibility mapping with different recurrent neural networks *Computational Geoscience* **138** 104445

[20]	Krizhevsky A, Sutskever I and Hinton G E 2017 ImageNet classification with deep convolutional neural networks *Communication of the ACM* **60** 84–90

[21]	Yin W, Kann K, Yu M and Schütze H 2017 Comparative Study of CNN and RNN for Natural Language Processing *ArXiv* **1702** 01923

[22]	Long J, Shelhamer E and Darrell T 2015 Fully convolutional networks for semantic segmentation *2015 IEEE Conference on Computer Vision and Pattern Recognition (CVPR)* (IEEE) pp 3431–40

[23]	Ghorbanzadeh O, Blaschke T, Gholamnia K, Meena S, Tiede D and Aryal J 2019 Evaluation of Different Machine Learning Methods and Deep-Learning Convolutional Neural Networks for Landslide Detection *Remote Sensing (Basel)* **11** 196

[24]	Guirado E, Tabik S, Alcaraz-Segura D, Cabello J and Herrera F 2017 Deep-learning Versus OBIA for Scattered Shrub Detection with Google Earth Imagery: Ziziphus lotus as Case Study *Remote Sensing (Basel)* **9** 1220

[25]	Yong Du, Wang W and Wang L 2015 Hierarchical recurrent neural network for skeleton based action recognition *2015 IEEE Conference on Computer Vision and Pattern Recognition (CVPR)* (IEEE) pp 1110–8

[26]	Sauter T, Weitzenkamp B and Schneider C 2010 Spatio-temporal prediction of snow cover in the Black Forest mountain range using remote sensing and a recurrent neural network *International Journal of Climatology* **30** 2330–41

[27]	Hashim M, Misbari S, Nadzri Md Reba M, Beirvand Pour A, Wei Jaw S, Zafirah Ab Lah N and Khairul Abdullah Halim M 2015 Satellite-based inventorying major landslides in kelantan river basin due to massive december 2014 flood episode *Asian Association on Remote Sensing* **6** 4732

[28] Pettorelli N, Vik J O, Mysterud A, Gaillard J-M, Tucker C J and Stenseth N Chr 2005 Using the satellite-derived NDVI to assess ecological responses to environmental change *Trends in Ecology & Evolution* **20** 503–10

[29] Ma Z and Mei G 2021 Deep learning for geological hazards analysis: Data, models, applications, and opportunities *Earth Science Review* **223** 103858

[30] Feng K, Hong H, Tang K and Wang J 2019 Decision Making with Machine Learning and ROC Curves *SSRN Electronic Journal* **1905** 02810